Dependence on pressure of the refractive indices of wurtzite ZnO, GaN, and AlN

A. R. Goñi,[1,2] F. Kaess,[3] J. S. Reparaz,[2,4] M. I. Alonso,[2] M. Garriga,[2] G. Callsen,[3] M. R. Wagner,[3,4]
A. Hoffmann,[3] and Z. Sitar[5]

[1]*ICREA, Passeig Lluís Companys 23, E-08010 Barcelona, Spain*
[2]*Institut de Ciència de Materials de Barcelona (ICMAB-CSIC), Esfera UAB, E-08193 Bellaterra, Spain*
[3]*Institut für Festkörperphysik, EW 5–1, Technische Universität Berlin, Hardenbergstr. 36, D-10623 Berlin, Germany*
[4]*Catalan Institute of Nanotechnology, Campus UAB, E-08193 Bellaterra, Spain*
[5]*Dept. of Materials Science and Engineering, North Carolina State University, Raleigh, North Carolina 27695-7919, USA*

We have measured both the ordinary and extraordinary refractive index of *m*-plane cuts of wurtzite ZnO, GaN, and AlN single crystals at room temperature and as a function of hydrostatic pressure up to 8 GPa. For that purpose we have developed an alternative optical interference method, called bisected-beam method, which leads, in general, to high contrast interference fringes. Its main feature, however, is to be particularly suitable for high pressure experiments with the diamond anvil cell, when the refractive index of the sample is low and similar to that of diamond and/or the pressure transmitting medium, as is the case here. For all three wide-gap materials we observe a monotonous decrease of the ordinary and extraordinary refractive indices with increasing pressure, being most pronounced for GaN, less marked for ZnO, and the smallest for AlN. The frequency dependence of the refractive indices was extrapolated to zero energy using a critical-point-plus-Lorentz-oscillator model of the ordinary and extraordinary dielectric function. In this way, we determined the variation with pressure of the electronic part (no-phonon contribution) of the static dielectric constant ε_∞. Its volume derivative, $r = d \ln \varepsilon_\infty / d \ln V$, serves as *single* scaling coefficient for comparison with experimental and/or theoretical results for other semiconductors, regarding the pressure effects on the dielectric properties. We have obtained an ordinary/extraordinary average value $\bar{r}$ of 0.49(15) for ZnO, 1.22(9) for GaN, and 0.32(4) for AlN. With the values for the ordinary and extraordinary case being within experimental uncertainty, there is thus no apparent change in dielectric anisotropy under pressure for these wurtzite semiconductors. Results are discussed in terms of the pressure-dependent electronic band structure of the materials.

I. INTRODUCTION

The complex dielectric function $\varepsilon(\omega) = \varepsilon_1(\omega) + i \cdot \varepsilon_2(\omega)$ is a fundamental material property which describes the way electromagnetic radiation interacts with the given substance. In particular, for photon energies $\hbar\omega$ below the fundamental band gap, the material is fully transparent (no optical absorption besides for that due to vibrations in the far infrared) and the frequency dependent refractive index is simply given by [1]:

$$n(\omega) = \sqrt{\varepsilon_1(\omega)}. \tag{1}$$

In fact, $\varepsilon_1(\omega)$ and thus $n(\omega)$ are second-rank tensors which, in wurtzite materials, possess only two independent components: the ordinary one, describing the dielectric response for electric fields polarized in the plane perpendicular to the hexagonal *c* axis, and the extraordinary component, corresponding to fields polarized parallel to *c*. In wide-gap semiconductors like ZnO and several group-III nitrides such as GaN and AlN, the refractive indices (n_{ord} and n_{ext}) play a key role, particularly, in the description of the waveguiding properties and, generally, for the design of optoelectronic devices [2,3]. Another important parameter is the electronic part (no-phonon contribution) of the static dielectric constant ε_∞, which enters in all charge screening effects and other collective phenomena like exciton formation, plasmons, etc. In addition, for strongly polar materials like ZnO, GaN, and AlN the dielectric constant ε_∞ is also determinant for several lattice-dynamical properties like, for example, the transverse effective charge e_T^*. The latter is at the origin of the LO-TO splitting between the frequencies of the longitudinal and transversal optical phonon modes [4].

Large built-in and/or residual strains are ubiquitous in nowadays micro and nano-optoelectronic devices and heterostructures due to the mandatory combination of materials with large lattice mismatch [5]. Hence the precise knowledge of the way in which the refractive index as well as ε_∞ vary upon mechanical stress is clearly an issue of relevance in semiconductor research. A case of particular interest concerns the typical difficulties that arise when trying to understand the volume dependence of the transverse effective charge e_T^* in polar semiconductors, if reliable values for the pressure coefficients of ε_∞ are lacking. The crucial point is that the behavior of e_T^* as a function of volume is not solely determined by the sign of the pressure coefficient of the LO-TO splitting, which can be either directly measured by Raman scattering or obtained from first-principles lattice dynamical calculations (see Refs. [6–9] for ZnO, Refs. [10–12] for GaN, and Refs. [11,13,14] for AlN). For the two nitrides the LO-TO splitting slightly increases with pressure [11], whereas for ZnO it decreases [9]. In contrast, the static dielectric constant ε_∞ as well as the transverse effective charge decrease in all three cases. In the general case, although e_T^* seems to exhibit a systematics in terms of the polarity of the lattice or the bond ionicity [9], this does not hold for the sign and magnitude of the pressure derivative of ε_∞ and LO-TO splitting. Even more intriguing is the apparent total lack of correlation between the pressure coefficients of the two latter material properties.

In this work we report the dependence on hydrostatic pressure of the refractive indices (ordinary as well as extraordinary) of the wurtzite phases of three wide-gap semiconductors,

namely ZnO, GaN, and AlN. Measurements were performed with the diamond anvil cell for pressures up to 8 GPa in the spectral range from roughly 1.4 to 2.6 eV, using the purposely developed interferometric method of the bisected beam. We use a Lorentz oscillator plus a P_0-type critical-point model of the dielectric function to fit the experimental data, in order to obtain by extrapolation the values of ε_∞ and its pressure dependence. In an attempt to look for specific trends in the volume dependence of ε_∞, we have performed an exhaustive survey of the literature and compared experimental and/or theoretical results for different semiconductors spanning the whole range of bond ionicities, from homopolar elemental semiconductors up to ionic insulators.

II. EXPERIMENT

All samples studied here are high quality single crystals of the wurtzite phase. The two ZnO crystals (one *c*-plane and one *m*-plane crystal cut) were grown by hydrothermal methods and purchased from CrysTec. The GaN sample (*m*-plane cut), provided by the Ferdinand-Braun-Institut, Berlin, was grown by hydride vapor phase epitaxy [15]. The AlN crystal (*m*-plane cut) was synthesized by the seeded crystal growth method utilizing physical vapor transport, as described elsewhere [16]. For optical interference experiments under high pressure, the samples were prepared by mechanical polishing in the form of plane-parallel plates with thicknesses ranging from 30 to 50 μm. To attain best possible contrast of the interference fringes after the initial coarse grinding, flat surfaces with optical quality were obtained by a series of polishing steps using alumina abrasive pastes with decreasing grain size (9 to 0.05 μm). The thinned samples were cut into pieces of approximately 150×150 μm^2 and loaded into a gasketed diamond-anvil cell (DAC) using a 4:1 mixture of methanol-ethanol as pressure-transmitting medium. Pressure was measured *in situ* by the ruby luminescence method [17].

A custom-made micro-optical system was used to focus white light from a tungsten lamp onto the sample inside the DAC and to collect the transmitted intensity, focusing it onto the slits of a 0.3 m single grating monochromator. The light was detected by a Si-based charge-coupled device (CCD) detector. Lines of a Hg-Ar lamp were used for the wavelength calibration. Spectroscopic ellipsometry measurements at ambient pressure-temperature conditions were performed in the range from 1.4 to 5.2 eV using a SOPRA ES4G ellipsometer. As excitation light source we used a 75 W high-pressure Xe arc lamp and the reflected light was collected by an optical fiber, coupled into a double prism/grating monochromator of 0.75 m equivalent focal length, and detected with a multialkali photomultiplier tube.

III. BISECTED-BEAM INTERFERENCE METHOD

The conventional optical interference method for the determination of the refractive index is based on the detection of the pattern of interference fringes, which develops when the main light beam transmitted through a plane-parallel plate interferes with its multiple reflections between both surfaces of the sample, leading to a series of intensity maxima and minima as a function of the wavelength of the transmitted light [18]. The contrast between maxima and minima is strongly reduced
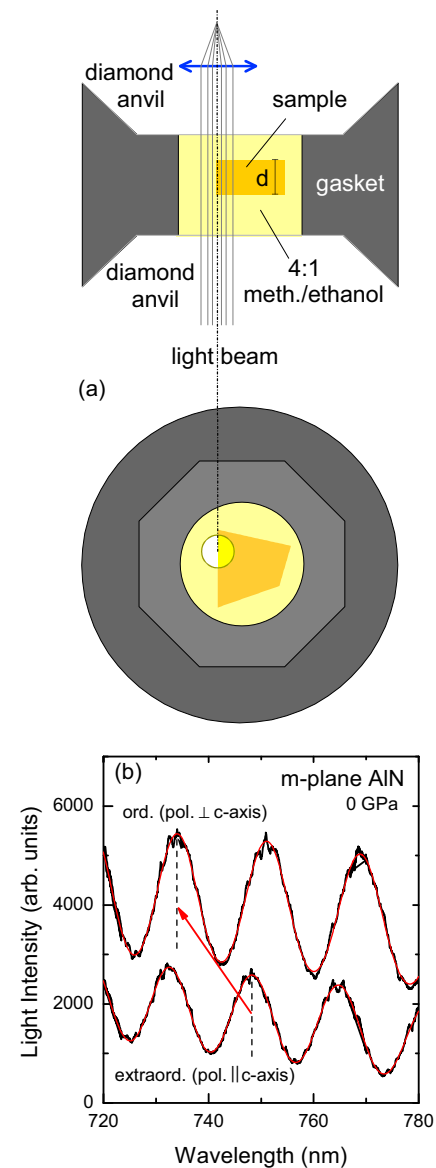
FIG. 1. (Color online) (a) Sketch of the optical path through the diamond anvil cell in the bisected-beam optical interference method. The upper and lower drawing corresponds to a cross sectional and front (transmission) view, respectively. (b) Transmission spectra (black lines) of a 47-μm-thick piece of *m*-plane AlN at nearly ambient pressure loaded into the DAC obtained with the bisected-beam method using linearly polarized light either perpendicular (ordinary) or parallel (extraordinary) to the crystallographic *c* axis. Only a small wavelength range is shown for clarity. Red curves represent results of a fit to determine the position of the interference maxima. Vertical dashed lines indicate a maximum in each spectrum with the same interference index *m*.

if the refractive index of the material is similar to the one of either the diamond anvils ($n_{\text{diamond}} = 2.4$) or the pressure medium ($n_{\text{alcohol}} = 1.3$ to 1.6 between 0 and 8 GPa). This is exactly the case for the three wide-gap semiconductors studied here. We thus developed the alternative interference method of the bisected beam, which does not rely on any dielectric contrast. As sketched in Fig. 1(a), the method consists in focusing the incident light onto a small spot of 50 to 100 μm

in diameter at one sharp cleaved edge of the sample, in such a way that roughly half of the beam is transmitted through the sample and the other half passes nearby through the pressure medium. By tightly focusing the bisected beam at the entrance of the optical fiber used to convey the light to the grating spectrometer, both beam halves interfere with each other leading to high contrast fringes. The conditions for constructive interference correspond to the cases in which the optical path difference between both beam halves is an integer multiple of the wavelength of the light, according to

$$n(\lambda_m) - n_{\text{med}}(\lambda_m) = \frac{m \cdot \lambda_m}{d}, \quad m \in \mathbb{Z}, \qquad (2)$$

where n, n_{med} are the refractive index of sample and pressure medium, respectively, d is the sample thickness, and λ_m is the wavelength of the interference maximum with index m.

The incident light beam can be linearly polarized at any desired angle just by placing a rotatable linear polarizer in the optical path before the DAC. For a m-plane crystal cut the crystallographic c axis lies in the plane of the sample surface, perpendicular to direction of incidence. Hence, simply by orienting the linear polarizer either perpendicular or parallel to the c axis, one can determine independently the ordinary and extraordinary refractive index of the sample, respectively. Figure 1(b) displays an example of transmission spectra (black lines) of a piece of m-plane AlN at nearly ambient pressure loaded into the DAC, obtained with the bisected-beam method using linearly polarized light properly oriented with respect to the c axis. The main oscillations correspond to the fringes resulting from the interference of both halves of the light beam. Red curves represent results of a fit to determine the position of the maxima. Vertical dashed lines indicate a maximum in each spectrum with the same interference index m; their relative wavelength shift being a direct consequence of the difference in ordinary and extraordinary refractive index [Eq. (2) holds for both cases but with slightly different wavelength].

The use of the bisected-beam method for the determination of the refractive index of a substance under high pressure, though, presents the difficulty that the spectral dependence of the refractive index of the pressure medium, as well as its variation with pressure, have to be well known. This appears as a serious limitation of the method. Fortunately enough, in the case of the 4:1 methanol-ethanol mixture, we can count on the results of the very meticulous work of Eggert *et al.* [19], in which the authors report on measurements of $n_{\text{alc}}(\omega, P)$ with a residual standard error of 4×10^{-3} for photon energies $\hbar\omega$ in the range from 1.5 to 3.0 eV and hydrostatic pressures P between 0.5 and 11.5 GPa. The relevant equations are [20]

$$n_{\text{alc}}(\omega, P) = \left(1 + \frac{E_d \cdot E_0}{E_0^2 - (\hbar\omega)^2}\right)^{\frac{1}{2}}, \qquad (3)$$

$$E_d = 10.6 \left(\frac{\rho}{\rho_0}\right)^{1.31}, \quad E_0 = 13.4 \left(\frac{\rho}{\rho_0}\right)^{0.07}, \qquad (4)$$

$$\frac{\rho}{\rho_0} = \left[1 - \frac{1}{B_0' + 1} \cdot \ln\left(1 + \frac{(B_0' + 1) \cdot P}{B_0}\right)\right]^{-1}, \qquad (5)$$

where $B_0 = 0.778$ GPa and $B_0' = 10.18$ are the bulk modulus of the methanol-ethanol mixture and its pressure derivative, respectively (see discussion in Ref. [19]).

We point out that condensed He is an alternative pressure medium which presents the great advantage of having an almost dispersionless refractive index that might be also fairly insensitive to pressure. Nevertheless, it presents disadvantages too. First of all, the preceding statement has to be corroborated experimentally by performing a similar study as for the methanol-ethanol mixture. More important is perhaps the fact that condensed He needs to be loaded into the DAC following a cumbersome cryogenic procedure which is extremely time and resources consuming. Cryogenic He loading, though, can be circumvented by employing membrane DACs, which is not our case.

IV. RESULTS AND DISCUSSION

A. Measurements of the refractive index under pressure

Figure 2 displays two representative transmission spectra of a c-plane ZnO sample measured at different pressures, where the interference patterns are readily observed. The zero-pressure spectrum was actually taken using the bisected-beam method with the sample already loaded into the DAC, thus immersed in alcohol. The pressure cell, though, was very loosely closed such that the residual pressure is estimated to be less than 0.03 GPa. The wavelength λ_m of each interference maximum of order m is obtained with precision by fitting the fringes with Gaussians, as illustrated by the red curves in Fig. 1(b). To determine the order m of each interference maximum and the sample thickness d_0 from the zero-pressure spectrum, we need the values of the refractive index of the sample at ambient pressure. For this purpose we have previously determined both ordinary and extraordinary refractive indices as a function of photon energy for the three materials (using the m-plane cuts) by means of spectroscopic
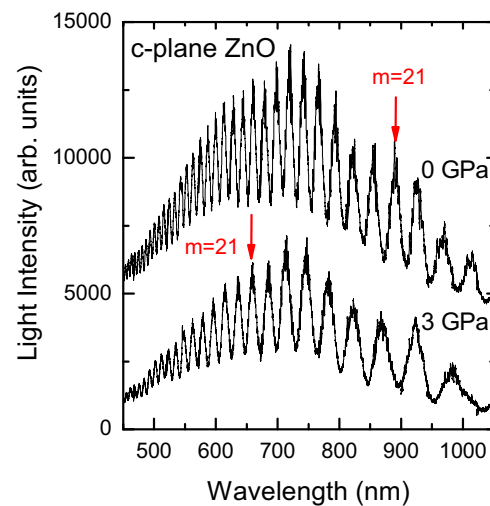
FIG. 2. (Color online) Two representative transmission spectra of a 31-μm-thick piece of c-plane ZnO measured at room temperature for different hydrostatic pressures. The interference maximum with index $m = 21$ is shown to shift to shorter wavelengths with increasing pressure.

ellipsometry. In this way and using Eqs. (3) to (5) for the refractive index of the alcohol mixture, we obtain

$$m = \frac{\lambda_{m+1} \cdot \Delta n(\lambda_m)}{\lambda_m \cdot \Delta n(\lambda_{m+1}) - \lambda_{m+1} \cdot \Delta n(\lambda_m)},$$

$$\Delta n(\lambda) = n(\lambda) - n_{\text{alc}}(\lambda), \quad (6)$$

$$d_0 = \frac{1}{N} \sum_m \frac{m \cdot \lambda_m}{\Delta n(\lambda_m)}, \quad (7)$$

where m is actually the integer part of Eq. (6) and d_0 is the average value obtained from the N maxima considered. It is crucial to keep track of the numbering of the maxima during the whole pressure cycle (see example of Fig. 2 for $m = 21$). This was achieved by monitoring the movement of a certain maximum live at the CCD camera, while pressure was slowly changed employing an electric motor drive with a speed of $\sim$0.1 GPa/min. The results obtained for the refractive indices of ZnO, GaN, and AlN are shown in Figs. 3(a) to 3(c) as a function of photon energy and, for the sake of clarity, only for selected pressures. Closed (open) symbols correspond to the ordinary(extraordinary) refractive index data.

For the correct analysis of the high-pressure transmission spectra, it is important to take into account the thickness reduction of the sample by properly scaling d using a Murnaghan-type pressure-volume equation of state [21]. The key point is that in wurtzite materials the ratio between the length of the crystallographic c and a axes may vary linearly with pressure (as the bulk modulus B does). In this case, the thickness scales differently with pressure for a c-plane or an m-plane sample. By defining $R = \frac{c}{a}$, $R_0 = \frac{c_0}{a_0}$, and $R'_0 = \frac{d(\frac{c}{a})}{dP} = \frac{dR}{dP}$ and assuming that $R = R_0 + R'_0 \cdot P$ and $B = B_0 + B'_0 \cdot P$, we obtain that

$$\frac{a}{a_0} = \left(\frac{R}{R_0}\right)^{-\frac{1}{3}} \cdot \left(1 + \frac{B'_0}{B_0} \cdot P\right)^{-\frac{1}{3B'_0}} \equiv \frac{d}{d_0} \quad (m \text{ plane}), \quad (8)$$

$$\frac{c}{c_0} = \left(\frac{R}{R_0}\right)^{+\frac{2}{3}} \cdot \left(1 + \frac{B'_0}{B_0} \cdot P\right)^{-\frac{1}{3B'_0}} \equiv \frac{d}{d_0} \quad (c \text{ plane}). \quad (9)$$

The used values of the c/a ratio, the bulk modulus, and their pressure derivatives are listed in Table I for the three studied materials.

A first test of the suitability of the presented method consisted in comparing the results obtained for the ordinary

TABLE I. Bulk modulus B_0 and its pressure derivative B'_0 and the c/a crystallographic axes ratio and its pressure derivative for the wurtzite phases of ZnO, GaN, and AlN. Numbers in parentheses are error bars.

Material	B_0 (GPa)	B'_0	$R_0 = \frac{c_0}{a_0}$	$R'_0 = \frac{d(c/a)}{dP}$ (GPa^{-1})
ZnO	142.6(2)[a]	3.6[a]	1.6021(3)[a]	−0.0005(1)[a]
GaN	200(20)[b]	4.3(20)[c]	1.626(4)[c]	0[c]
AlN	208(6)[d]	6.3(9)[d]	1.601(2)[d]	−0.0006(1)[d]

[a]Reference [22].
[b]Reference [23].
[c]Reference [24].
[d]Reference [25].
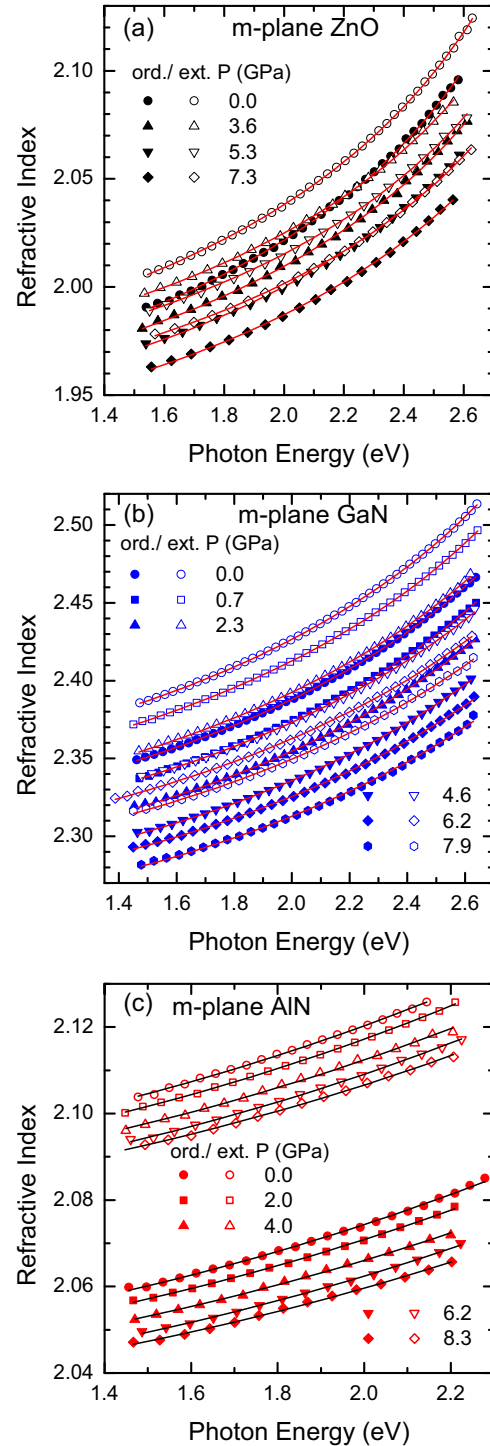
FIG. 3. (Color online) Ordinary (closed symbols) and extraordinary (open symbols) refractive index of (a) ZnO, (b) GaN, and (c) AlN as a function of photon energy at several hydrostatic pressures. The solid curves represent least-squares fits to the experimental data using a simple model consisting of one Lorentz oscillator and one P_0-type critical point (see text for details).

refractive index of ZnO using either a c-plane cut and unpolarized light or an m-plane sample and linearly polarized light along the direction perpendicular to the crystallographic c axis. Figure 4 shows both data sets of n_{ord} versus pressure for
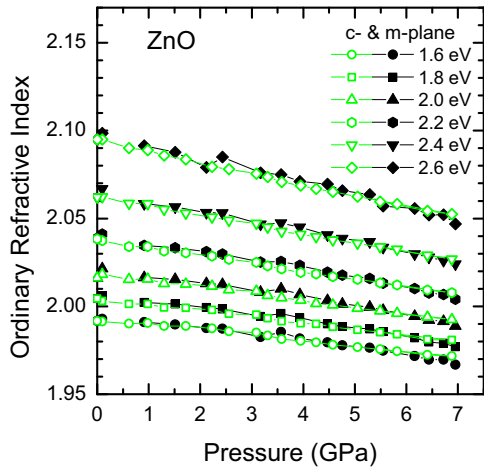
FIG. 4. (Color online) Comparison of the results obtained for the pressure dependence of the ordinary refractive index of ZnO using either a c-plane (green, open symbols) or an m-plane (black, closed symbols) crystal cut. The data points correspond to the values of $n_{\rm ord}$ at the photon energies indicated in the legend.

different photon energies in the case of the c-plane (green, open symbols) and the m-plane sample (black, closed symbols), exhibiting excellent agreement with each other. We emphasize that such good agreement was attained only after the correct pressure dependence of the sample thickness was considered, as expressed in Eqs. (8) and (9).

B. Model dielectric function

After Eq. (1), for a description of the photon-energy dispersion of the refractive index, it is sufficient to be able to set up a model dielectric function for $\varepsilon_1(\omega)$ that can be successfully fitted to the experimental data points in the spectral region of transparency of the material, i.e., below the fundamental band-gap energy. In this respect, the main constraint for the model dielectric function is that it should fulfill the so-called static sum rule (see, for instance, Appendix A of Ref. [26]):

$$\varepsilon_1(\omega = 0) \equiv \varepsilon_\infty = 1 + \frac{2}{\pi} \cdot \int_0^{E_c} \frac{\varepsilon_2(\omega)}{\omega} d\omega, \qquad (10)$$

where the cutoff energy E_c is introduced to avoid the unphysical extension of the dielectric response to higher energies within the model. Equation (10) is a direct consequence of the requirements of causality to the optical response function, which mathematically means that its frequency-dependent real and imaginary parts are related via the Kramers-Kronig relations [1]. Moreover, the static sum rule is intimately related to the total oscillator sum rule, which expresses the fact that the addition of the contributions to the imaginary part of the dielectric function $\varepsilon_2(\omega)$ from all electronic interband transitions should be finite and give the effective number of valence electrons participating in the optical response [26]. Both sum rules are extremely powerful relations which, in turn, leave sufficient freedom for the construction of the model dielectric function. Models of different complexity might differ much in their spectral line shape above the fundamental absorption edge and still yield the correct static limit and a

low-frequency dispersion in agreement with the experimental one (see, for instance, Refs. [27–29]).

In order to set up the model we make explicit use of the measured real and imaginary parts of the dielectric function determined by means of spectroscopic ellipsometry in a very wide range of photon energies from the visible up to the deep ultraviolet (see Ref. [30] for ZnO, Refs. [31,32] for GaN, and Refs. [31,33] for AlN). A careful inspection of the imaginary part $\varepsilon_2(\omega)$ indicates that the leading contribution at low frequencies stems from an extended critical point located at an energy E_1 between 6 and 8 eV. It turns out that such a strong feature in the dielectric response corresponds to a two-dimensional critical point of P_0 type [34], for which both valence and conduction bands run parallel partly along a given high symmetry direction in the Brillouin zone. This single critical point, however, cannot yield a fully satisfactory description of the measured refractive-index dispersion at photon energies closer to the absorption edge. To account for this extra dispersion we added one Lorentz oscillator, associated with interband transitions at an energy E_0 close to the fundamental gap. We notice that the sharp peak at the absorption edge in $\varepsilon_2(\omega)$ [30,31], which is attributed to the discrete exciton at the direct gap E_0, is perfectly described by a Lorentzian peak [28]. This feature can be observed at room temperature due to the very large exciton binding energies in these wide-gap materials, partly because of the small static dielectric constant (poor screening of the Coulomb interaction). Within this model, the refractive index is expressed as [28,35]

$$n^2(\omega, P) = 1 + A(P) \cdot \frac{\gamma \cdot [\hbar\omega - E_0(P)]}{[\hbar\omega - E_0(P)]^2 + \gamma^2} - B(P) \cdot$$
$$\times \left[\frac{E_1(P)}{\hbar\omega} \right]^2 \cdot \ln \left(\frac{1 - \left[\frac{\hbar\omega}{E_1(P)} \right]^2}{1 - \left[\frac{\hbar\omega}{E_c} \right]^2} \right). \qquad (11)$$

The first nontrivial term corresponds to the Lorentz oscillator centered at E_0 with linewidth γ and amplitude A. The last term in Eq. (11) represents the contribution of the P_0-type critical point at an energy E_1 and with amplitude B. A quick look at $\varepsilon_2(\omega)$ indicates that a cutoff energy of $E_c = 20$ eV seems appropriate for the three materials considered. As far as the exciton linewidth is concerned, we just set it to a value of $\gamma = 0.01$ eV, which is a typical room-temperature exciton broadening. We further consider that γ is independent of pressure [36,37]. This assumption is not only supported by experimental evidence, it is certainly correct for all practical means, since the fit of the refractive index data is not sensitive to the particular value of γ in view of the fact that the difference between the highest photon energy in the experiment and E_0 is much larger than the linewidth. The particular choice of γ just changes the initial value of the amplitude A, having no influence on the quality of the fit.

In this way, the model function has, in principle, only four adjustable parameters remaining, which are also pressure dependent. Unfortunately, it turned out that the nonlinear least-squares fitting routine would not converge to a minimum due to a strong correlation between the pair of energies and the pair of amplitudes of both oscillators. We decided then to fix the values of the parameters of the Lorentz oscillator

TABLE II. List of parameters and their pressure dependence as obtained from fits of the model dielectric function given by Eq. (11) to the ordinary and extraordinary $n(\omega)$ data at different pressures for the wurtzite phases of ZnO, GaN, and AlN. They are the energy positions E_0, E_1 and amplitudes A, B of the Lorentz oscillator and the P_0-type critical point, respectively. For the fits a common oscillator linewidth $\gamma = 0.01$ eV and a cutoff energy $E_c = 20$ eV were used. Data from the literature are properly indicated. Numbers in parentheses are error bars.

| Material (wurtzite) | $E_0 = a + b \cdot P + c \cdot P^2$ | | | $A = a\left(\frac{E_0(P)}{E_0}\right)^{1.5}$ | $E_1 = a + b \cdot P$ | | $B = a + b \cdot P$ | |
	a (eV)	b (eV/GPa)	c (eV/GPa^2)	a	a (eV)	b (eV/GPa)	a	b (GPa^{-1})
ZnO (ord.)	3.441(1)[a]	0.0247(1)[a]		−90.8(6)	7.46(4)	0.188(9)	3.09(1)	0.015(3)
(extraord.)	3.482(1)[a]	0.0268(1)[a]		−96.5(6)	7.25(4)	0.185(8)	3.12(1)	0.012(2)
GaN (ord.)	3.450(5)	0.0432(6)[b]	−0.0004(1)[b]	−53.0(20)	5.95(10)	0.065(4)	4.61(1)	−0.031(4)
(extraord.)	3.472(5)	0.0432(6)[b]	−0.0004(1)[b]	−69.5(15)	6.05(10)	0.068(5)	4.75(2)	−0.028(3)
AlN (ord.)	6.20(1)[c]	0.037[a]			7.70(4)	0.066(9)	3.73(1)	0.004(2)
(extraord.)	5.97(1)[e]	0.037[d]			7.36(5)	0.054(9)	3.87(1)	0.003(2)

[a]Reference [36].
[b]Reference [37].
[c]Reference [42].
[d]Reference [43].
[e]Reference [44].

according to the following criteria: E_0 was identified as the corresponding fundamental band gap and its value at ambient pressure and its pressure coefficient were taken from experimental results of the literature. The amplitude $A(0)$ at zero pressure was obtained from a fit of the refractive index data from ellipsometry, extending the fit up to photon energies close to the gap. Furthermore, due to the outspoken excitonic character of the optical transitions at E_0, we expect the oscillator amplitude A to be proportional to the excitonic oscillator strength [38]. The latter varies, within Elliott's theory of the exciton absorption [39], as $E_0^{3/2}$. The dependence on pressure of the amplitude parameter A was thus calculated as

$$A(P) = A(0) \cdot \left[\frac{E_0(P)}{E_0(0)}\right]^{\frac{3}{2}}. \tag{12}$$

We note that such pressure dependence was already demonstrated to hold for the excitonic absorption edge of GaAs [40] and Ge [41]. In conclusion, the only free parameters of the model used to fit the energy dispersion of the refractive index under high pressure are the amplitude and energy position of the critical point oscillator. We point out that the P_0-type critical point is not only the leading term in Eq. (11) but also the logarithmic dependence of its contribution is crucial for attaining a good description of the refractive index dispersion.

In wurtzite semiconductors, the top of the valence band at the Brillouin zone center (the Γ point) splits into three twofold degenerate bands labeled as A, B, and C in decreasing energy order, all of which posses pure atomic p character. These wave functions can be classified according to the eigenvalues of the total angular momentum **J** as $|J, \pm J_z\rangle = |\frac{3}{2}, \pm \frac{3}{2}\rangle, |\frac{3}{2}, \pm \frac{1}{2}\rangle$, and $|\frac{1}{2}, \pm \frac{1}{2}\rangle$. The bottom of the conduction band, in contrast, has pure atomic s character. Within the dipolar approximation, the optical transitions contributing to the ordinary or the extraordinary dielectric function are the ones involving the valence band $|\frac{3}{2}, \pm \frac{3}{2}\rangle$ and mainly $|\frac{1}{2}, \pm \frac{1}{2}\rangle$ multiplets, respectively. The precise assignment of each multiplet to the valence bands A to C depends strongly

on the strength of the spin-orbit interaction and crystal field, being thus different in every material. As seen in Table II, the difference between the values of the fundamental gap E_0 corresponding to the ordinary and extraordinary case varies for each material, according to the literature, whereas the pressure coefficient does not. In the same table, the parameters corresponding to the P_0-type critical point are also listed. They were obtained by fitting Eq. (11) to the refractive-index data points using solely B and E_1 as adjustable parameters. The solid curves in Figs. 3(a) to 3(c) represent the results of the fits. The description of the dispersion of the refractive index as a function of pressure in terms of Eq. (11) is in all cases excellent. In the case of AlN, the fundamental gap E_0 is also as large as E_1 [45]. This might be the reason for the fact that only the leading term corresponding to the critical point at E_1 was necessary to effectively fit the refractive index data. We thus have dropped the contribution of the Lorentz oscillator in the case of AlN.

Figures 5(a) and 5(b) display the fitted values of the critical point energy E_1 and amplitude B, respectively, as a function of pressure for all three materials. The E_1 values fall all in the range from approximately 6 to 7.5 eV. For a tentative identification of the interband optical transitions contributing to that critical point at E_1, it is instructive to inspect the electronic band structure of the three semiconductors, looking for the regions in the Brillouin zone where valence and conduction band run piecewise parallel to each other, having the desired gap energy. For ZnO this occurs along the Γ-A direction close to both ends, i.e., the zone center and the A point [46], whereas for the nitrides this happens along the Γ-M direction close to the zone edge [43]. Due to the 2D nature of this critical point, we expect the amplitude parameter B to be proportional to the extension of the wave vector segment in the Brillouin zone for which the valence and conduction band run parallel. Under pressure, any change in B would, thus, be ascribed to a variation of such extension.

For the three materials E_1 turns out to increase linearly with pressure. This is the main reason for the general decrease of
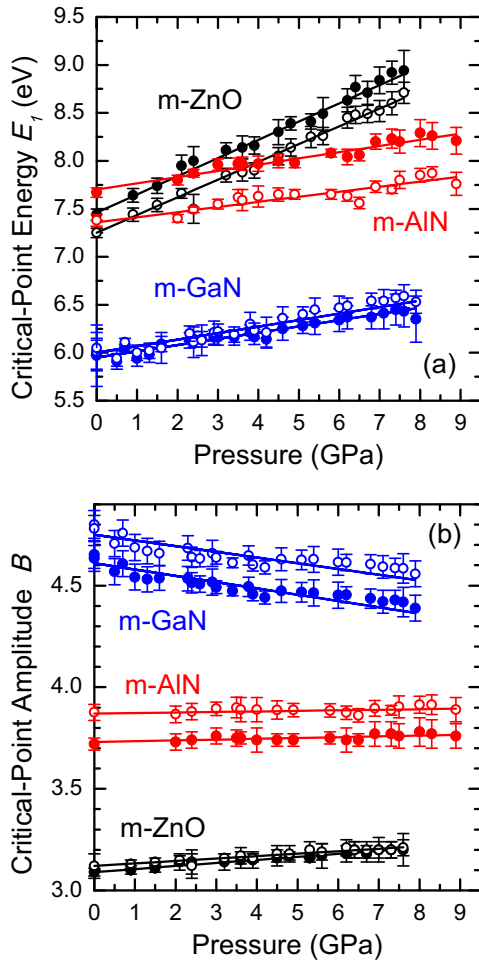
FIG. 5. (Color online) Variation with pressure of (a) the critical point energy E_1 and (b) the amplitude B, as obtained by fitting the photon-energy dependence of the ordinary (closed symbols) and extraordinary (open symbols) refractive index data of ZnO (black), GaN (blue), and AlN (red), using the model dielectric function given by Eq. (11). Curves represent least-squares fits to the data points using linear expressions.

FIG. 6. (Color online) (a) Dependence on pressure of the ordinary (closed symbols) and extraordinary (open symbols) electronic part of the static dielectric constant ε_∞ and (b) double-logarithmic plot of ε_∞ versus volume both for ZnO (black), GaN (blue), and AlN (red), using Eq. (13) to extrapolate the frequency dependence of $n_{\text{ord/ext}}(\omega)$ to zero energy. Curves represent least-squares fits to the data points using linear or quadratic expressions.

the refractive indices with increasing pressure. In the case of GaN, the amplitude B of the critical-point oscillators (ordinary as well as extraordinary) displays a decrease with increasing pressure. This behavior results in a much more pronounced pressure-induced reduction of the refractive indices, as observed in Fig. 3(b). For ZnO, in turn, the strong blueshift of E_1 with pressure seems to be partially compensated by the increase of the amplitude B, leading to a very moderate decrease of the refractive indices. For AlN E_1 shifts to higher energies the same way as for GaN but B is essentially pressure independent. The consequence is that the refractive indices of AlN decrease really slowly with increasing pressure.

C. Electronic static dielectric constant ε_∞

Besides the purpose of having a good description of the refractive index dispersion under high pressure, the model function of Eq. (11) can be used to extract the values of ε_∞ by extrapolation to zero photon frequency (static limit). Whereas

the extrapolation of the Lorentzian is trivial, the last term in Eq. (11) presents some difficulties. The correct limit is found by taking the series expansion of the logarithmic function ($E_1/E_c \ll 1$) and keeping the first two nonvanishing terms when $\omega \to 0$. The procedure yields

$$\varepsilon_\infty(P) = 1 - \frac{A(P) \cdot \gamma}{E_0(P)} + B(P) \cdot \left[1 - \frac{E_1^2(P)}{E_c^2} \right]. \quad (13)$$

Figure 6(a) displays the variation with pressure of the ordinary and extraordinary static dielectric constant ε_∞, as obtained from Eq. (13) using the oscillator parameters extracted from the fits to the refractive index data using Eq. (11), for ZnO (black symbols), GaN (blue symbols), and AlN (red symbols). Solid curves represent least-squares fits to the data points using linear or quadratic functions. As expected, ε_∞ decreases with increasing pressure in all cases. Furthermore, for the three materials the dependence of the ordinary and extraordinary components is the same within experimental uncertainty. We thus conclude that the dielectric anisotropy is essentially independent of pressure in these wide-gap materials.

TABLE III. Pressure and volume coefficients of the refractive index $n(\omega = 0)$ and (electronic) static dielectric constant ε_∞, respectively, for a series of semiconductors with different ionicity values f_i, according to Refs. [47,48]. The bulk modulus B_0 is used to transform from pressure to volume derivatives. The crystal structure of each material is indicated in parentheses, where d, zb, w, and rs stands for the diamond, zinc-blende, wurtzite, and rocksalt phase, respectively. For the anisotropic wurtzite materials the values in square brackets correspond to the extraordinary case. Numbers in parentheses are error bars.

Material	f_i	B_0 (GPa)	ε_∞	$\frac{dn(\omega=0)}{dP}$ (10^{-2} GPa^{-1})	$r = \frac{d\ln\varepsilon_\infty}{d\ln V}$	Ref.
Si (d)	0	95.8	12.05	−0.46	0.25	Theo.: Ref. [49], *ab initio* LMTO
					1.38	Theo.: dielectric theory, Eq. (15)
Ge (d)	0	74.4	15.94(2)	−4.5(2)	1.58(3)	Expt.: Ref. [28], transmission, DAC
		71.0	15.58	−4.03	1.43	Theo.: Ref. [49], *ab initio* LMTO
					1.41	Theo.: dielectric theory, Eq. (15)
GaAs (zb)	0.31	74.7	10.92(2)	−1.3(1)	0.73(4)	Expt.: Ref. [28], transmission, DAC
		74.2	10.83	−1.72	0.77	Theo.: Ref. [49], *ab initio* LMTO
					0.89	Theo.: dielectric theory, Eq. (15)
GaP (zb)	0.37	88.1	9.50(1)	−1.1(2)	0.63(8)	Expt.: Ref. [27], transmission, DAC
					0.79	Theo.: dielectric theory, Eq. (15)
AlN (w)	0.45	208	4.175(3) [4.349(3)]	**−0.17(2)** [**−0.15(2)**]	**0.34(4)** [**0.29(3)**]	Expt.: This work, transmission, DAC
					0.4[a]	Theo.: Ref. [50], *ab initio* pseudopot.
			4.2[a]	−0.37[a]	0.75[a]	Theo.: Ref. [43], *ab initio* LMTO
		203	4.227	−0.17	0.31	Theo.: Ref. [51], *ab initio* pseudopot.
					0.57	Theo.: dielectric theory, Eq. (15)
GaN (w)	0.47	200	5.346(12) [5.515(14)]	**−0.70(5)** [**−0.72(7)**]	**1.21(7)** [**1.23(11)**]	Expt.: This work, transmission, DAC
		245[b]		−0.69(8)	1.20(15)	Expt.: Ref. [52], transmission, DAC
					0.8[a]	Theo.: Ref. [50], *ab initio* pseudopot.
			5.4[a]	−0.44[a]	0.76[a]	Theo.: Ref. [43], *ab initio* LMTO
		176	5.673	−0.57	0.83	Theo.: Ref. [51], *ab initio* pseudopot.
					0.58	Theo.: dielectric theory, Eq. (15)
InN (w)	0.51	143[c]	8.4[a]	−1.25[a]	1.24[a]	Theo.: Ref. [43], *ab initio* LMTO
					0.57	Theo.: dielectric theory, Eq. (15)
ZnSe (zb)	0.60	64.7	5.9	−0.28	0.15	Theo.: Ref. [55], *ab initio* APW + lo
					0.42	Theo.: dielectric theory, Eq. (15)
ZnS (zb)	0.63	78.0	5.20	−0.29(1)[d]	0.19(1)[d]	Expt.: Ref. [56], interferometry, $P < 0.7$ GPa
				−0.28	0.19	Theo.: Ref. [55], *ab initio* APW + lo
					0.36	Theo.: dielectric theory, Eq. (15)
ZnO (w)	0.65	142.6	3.921(5) [3.980(6)]	**−0.33(10)** [**−0.35(10)**]	**0.47(15)** [**0.50(15)**]	Expt.: This work, transmission, DAC
				−0.34(1)[d] [−0.35(1)][d]	0.49(1)[d] [0.50(1)][d]	Expt.: Ref. [57], interferometry, $P < 0.7$ GPa
					0.31	Theo.: dielectric theory, Eq. (15)
CdS (w)	0.71	68.8	5.31 [5.38]	−1.38(1)[d] [−1.36(1)][d]	0.82(1)[d] [0.81(1)][d]	Expt.: Ref. [57], interferometry, $P < 0.7$ GPa
					0.26	Theo.: dielectric theory, Eq. (15)
MgO (rs)	0.86	162.6	3.02[d]	−0.158(1)[d]	0.30(1)[d]	Expt.: Ref. [58], interferometry, $P < 0.7$ GPa
					0.04	Theo.: dielectric theory, Eq. (15)
NaCl (rs)	0.95	23.84	2.334(1)	1.16(1)	−0.36(1)	Expt.: Ref. [59], interferometry, DAC
					−0.05	Theo.: dielectric theory, Eq. (15)
CsI (rs)	0.97	12.67	3.037(1)	3.74(2)	−0.54(1)	Expt.: Ref. [59], interferometry, DAC
					−0.08	Theo.: dielectric theory, Eq. (15)

[a]Effective values calculated as $(\varepsilon_\infty^{\text{ext}} + 2\varepsilon_\infty^{\text{ord}})/3$.
[b]Reference [53].
[c]Reference [54].
[d]Values at $\lambda = 589$ nm.

Figure 6(b) shows the dependence of ε_∞ on volume, depicted as double-logarithmic plot. Usually, this kind of representation leads to linear ε_∞-versus-volume relations, for which there suffices a single scaling coefficient (minus its slope $r = \frac{d\ln\varepsilon_\infty}{d\ln V}$) to describe the volume dependence of the dielectric constant. The values of r obtained for the three studied materials are listed in Table III together with experimental and/or theoretical results for the other eleven semiconductors. For ZnO we find good agreement between our values of r and the ones measured in a much smaller pressure range ($P < 0.7$ GPa) [57]. Nevertheless, we point out that ZnO is somewhat singular in the sense that its volume dependence of ε_∞ is nonlinear even in a double-logarithmic plot. A closer look at the data in Fig. 6(b) indicates that there are two regimes for lower and higher volume ratios than $\frac{V}{V_0} \sim 0.975$ characterized by a coefficient $r = 0.34(8)$ and $0.62(10)$, respectively (this holds for both the ordinary and extraordinary component). The reason for such a behavior remains elusive. Moreover, there are no theoretical values with which to compare. For GaN there is excellent agreement with previous experimental work regarding the ordinary component [52], whereas the theoretical values of r are about 30% lower [43,50]. For AlN we can only confront our values with theoretical results, finding good agreement with *ab initio* pseudopotential calculations [50,51].

An inspection of the r values listed in Table III, where data for fourteen semiconductors spanning all the range of possible ionicities are tabulated, clearly indicates that the volume dependence of ε_∞ depends on how covalent or ionic is the material. The bond ionicity f_i is defined according to the dielectric theory of the covalent bond of Phillips and Van Vechten [47], after which the static dielectric constant is given by

$$\varepsilon_\infty = 1 + D \cdot A \cdot \frac{\omega_p^2}{E_g^2}, \quad E_g^2 = E_h^2 + C^2, \qquad (14)$$

where ω_p is the valence-electron plasma frequency and E_g is the average optical gap or Penn gap, which splits into a homopolar or covalent contribution E_h and an ionic one C [60]. The bond ionicity is thus defined as $f_i = \frac{C^2}{E_g^2}$ [47]. Based on Eq. (14), we have derived before an approximate expression for r [26,28]

$$r = \frac{d\ln\varepsilon_\infty}{d\ln V} \approx \frac{5(\varepsilon_\infty - 1)}{3\varepsilon_\infty} \cdot (0.9 - f_i). \qquad (15)$$

Hence there should be a borderline between covalent and ionic behavior at $f_i = 0.9$, such that for lower (higher) ionicity the dielectric constant decreases (increases) with increasing pressure. Representative experimental as well as theoretical values of r taken from Table III for the fourteen listed semiconductors are plotted in Fig. 7 as a function of bond ionicity f_i. At first glance, expression (15), represented by the black closed symbols joined by full lines in Fig. 7, provides a nice description of the very general tendency of the volume derivative of the static dielectric function to decrease in magnitude with increasing bond ionicity, changing sign at a value of about 0.9. Equation (15) also seems to hold well for semiconductors of the same row of the Periodic Table such as Ge, GaAs, and ZnSe, predicting a reduction of r with increasing bond ionicity. In contrast, the data in
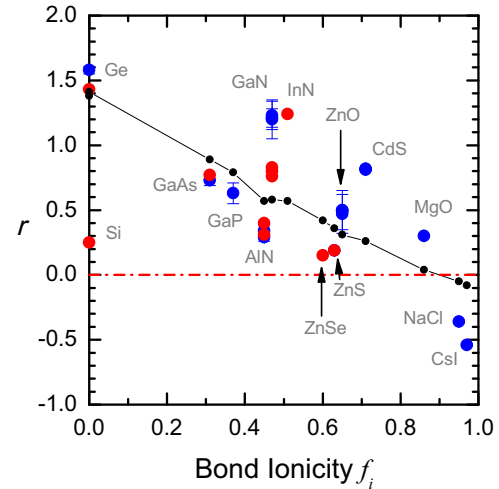
FIG. 7. (Color online) Values of the logarithmic volume derivative of the static dielectric constant, $r = \frac{d\ln\varepsilon_\infty}{d\ln V}$, as obtained from the entries in Table III, plotted as a function of the bond ionicity f_i for fourteen semiconductors. Blue symbols with error bars and red symbols correspond to experimental and theoretical results, respectively. Black dots joined by full lines represent the r values obtained within the dielectric theory of the covalent bond using Eq. (15).

Fig. 7 exhibit material trends for which expression (15) is totally unable to account for. For instance, it fails blatantly for materials with common cation (ZnSe, ZnS, ZnO, for example) or common anion (e.g., the nitrides), for which r increases with increasing ionicity instead. Also Eq. (15) is totally unable to explain the huge difference in the r values between Si and Ge, two homopolar semiconductors. The reason is simply that the bond ionicity, though important, is not the only factor to be taken into account at describing the volume dependence of the dielectric constants of a material. For each case, a discussion of the changes induced by pressure on the electronic band structure, in particular, interband transition energies and oscillator strengths, is unavoidable.

In order to understand the behavior of the dielectric function under pressure we consider its (microscopic) expression obtained within the dipolar approximation for electronic interband optical transitions, which can be written as [26,61]

$$\varepsilon_\infty - 1 \propto \rho \cdot \sum_i \frac{\mathbf{f}_{0i}}{(\hbar\omega)^2 - E_i^2}, \qquad (16)$$

where ρ is the density of polarizable units or dipoles and $\mathbf{f}_{0i}$ is the optical-dipolar strength of the ith oscillator with energy E_i. For ionic semiconductors ($f_i > 0.9$), the optical gap energy is mainly determined by its ionic part C and both pressure derivatives of C (i.e., E_i) and the oscillator strength $\mathbf{f}_{0i}$ are practically zero [26], due to the vanishing overlap between electronic wave functions of neighboring atoms. Thus Eq. (16) indicates that the behavior of the dielectric constant under pressure is primarily determined by the increase of the material density, leading to negative values of r. In covalently bonded semiconductors, in contrast, the increase in density under compression is overcompensated by the strong blueshift of the optical gaps, which appear in the denominator of Eq. (16).

Hence ε_∞ decreases under pressure and r is positive. The actual value of the logarithmic volume derivative r would finally depend on the sign and magnitude of the pressure coefficient of the oscillator strength. These, in turn, result from the peculiarities of the band structure of the material and its changes with pressure. Particularly for the critical-point oscillator at E_1, the reduction or enhancement of its oscillator strength is directly related to a pressure-induced reduction or enlargement of the Brillouin-zone segment along which valence and conduction band run parallel to each other.

V. SUMMARY

In summary, we have determined the dependence on pressure of both the ordinary and extraordinary refractive indices of the three wide-gap, strongly polar materials ZnO, GaN, and AlN at room temperature and pressures up to 8 GPa, using the alternative bisected-beam interferometric method. For all three semiconductors the refractive indices decrease monotonically with increasing pressure, whereas their dielectric anisotropy remains essentially unchanged. The electronic part of the static dielectric constant ε_∞ was extrapolated to zero energy from the refractive index dispersion using an empirical critical-point/oscillator model. The volume dependence of the static dielectric constant has been described by a single scaling coefficient $r = \frac{d \ln \varepsilon_\infty}{d \ln V}$ and compared to that of the other eleven semiconductors with different bond ionicity. Results were interpreted in terms of the pressure dependence of the electronic band structure and the concomitant changes in the optical properties of each material. In this way, we have provided deeper insight into the problem of the variation at reduced volume of charge-screening effects in semiconductors and insulators.

[1] C. F. Klingshirn, *Semiconductor Optics* (Springer, Berlin, 1997), p. 65.

[2] Ü. Özgür, Ya. I. Alivov, C. Liu, A. Teke, M. A. Reshchikov, S. Doğan, V. Avrutin, S.-J. Cho, and H. Morkoç, J. Appl. Phys. **98**, 041301 (2005).

[3] O. Ambacher, J. Phys. D: Appl. Phys. **31**, 2653 (1998).

[4] P. Y. Yu and M. Cardona, *Fundamentals of Semiconductors* (Springer, Berlin, 1996), p. 293.

[5] D. Zhu, D. J. Wallis, and C. J. Humphreys, Rep. Prog. Phys. **76**, 106501 (2013).

[6] F. J. Manjón, K. Syassen, and R. Lauck, High Press. Res. **22**, 299 (2002).

[7] F. Decremps, J. Pellicer-Porres, A. M. Saitta, J.-C. Chervin, and A. Polian, Phys. Rev. B **65**, 092101 (2002).

[8] J. Serrano, A. H. Romero, F. J. Manjón, R. Lauck, M. Cardona, and A. Rubio, Phys. Rev. B **69**, 094306 (2004).

[9] J. S. Reparaz, L. R. Muniz, M. R. Wagner, A. R. Goñi, M. I. Alonso, A. Hoffmann, and B. K. Meyer, Appl. Phys. Lett. **96**, 231906 (2010).

[10] P. Perlin, T. Suski, J. W. Ager, III, G. Conti, A. Polian, N. E. Christensen, I. Gorczyca, I. Grzegory, E. R. Weber, and E. E. Haller, Phys. Rev. B **60**, 1480 (1999).

[11] A. R. Goñi, H. Siegle, K. Syassen, C. Thomsen, and J.-M. Wagner, Phys. Rev. B **64**, 035205 (2001).

[12] M. P. Halsall, P. Harmer, P. J. Parbrook, and S. J. Henley, Phys. Rev. B **69**, 235207 (2004).

[13] M. Kuball, J. M. Hayes, A. D. Prins, N. W. A. van Uden, D. J. Dunstan, Y. Shi, and J. H. Edgar, Appl. Phys. Lett. **78**, 724 (2001).

[14] F. J. Manjón, D. Errandonea, A. H. Romero, N. Garro, J. Serrano, and M. Kuball, Phys. Rev. B **77**, 205204 (2008).

[15] E. Richter, U. Zeimer, S. Hagedorn, M. Wagner, F. Brunner, M. Weyers, and G. Traenkle, J. Cryst. Growth **312**, 2537 (2010).

[16] P. Lu, R. Collazo, R. F. Dalmau, G. Durkaya, N. Dietz, B. Raghothamachar, M. Dudley, and Z. Sitar, J. Cryst. Growth **312**, 58 (2009).

[17] H. K. Mao, J. Xu, and P. M. Bell, J. Geophys. Res. **91**, 4673 (1986).

[18] M. Cardona, W. Paul, and H. Brooks, J. Phys. Chem. Solids **8**, 204 (1959).

[19] J. H. Eggert, L.-W. Xu, R.-Z. Che, L.-T. Chen, and J.-F. Wang, J. Appl. Phys. **72**, 2453 (1992).

[20] We reproduce here the necessary formulas to calculate $n_{alc}(\omega, P)$ because there is a very unfortunate misprint in the equations of Ref. [19].

[21] F. D. Murnaghan, Proc. Natl. Acad. Sci. USA **30**, 244 (1944).

[22] S. Desgreniers, Phys. Rev. B **58**, 14102 (1998).

[23] C. Kisielowski, J. Krüger, S. Ruvimov, T. Suski, J. W. Ager, III, E. Jones, Z. Liliental-Weber, M. Rubin, E. R. Weber, M. D. Bremser, and R. F. Davis, Phys. Rev. B **54**, 17745 (1996).

[24] M. Ueno, M. Yoshida, A. Onodera, O. Shimomura, and K. Takemura, Phys. Rev. B **49**, 14 (1994).

[25] M. Ueno, A. Onodera, O. Shimomura, and K. Takemura, Phys. Rev. B **45**, 10123 (1992).

[26] A. R. Goñi and K. Syassen, Semicond. Semimetals **54**, 247 (1998).

[27] K. Strößner, S. Ves, and M. Cardona, Phys. Rev. B **32**, 6614 (1985).

[28] A. R. Goñi, K. Syassen, and M. Cardona, Phys. Rev. B **41**, 10104 (1990).

[29] S. Shokhovets, R. Goldhahn, G. Gobsch, S. Piekh, R. Lantier, A. Rizzi, V. Lebedev, and W. Richter, J. Appl. Phys. **94**, 307 (2003).

[30] P. Gori, M. Rakel, C. Cobet, W. Richter, N. Esser, A. Hoffmann, R. Del Sole, A. Cricenti, and O. Pulci, Phys. Rev. B **81**, 125207 (2010).

[31] L. X. Benedict, T. Wethkamp, K. Wilmers, C. Cobet, N. Esser, E. L. Shirley, W. Richter, and M. Cardona, Solid State Commun. **112**, 129 (1999).

[32] C. Cobet, R. Goldhahn, W. Richter, and N. Esser, Phys. Status Solidi B **246**, 1440 (2009).

[33] E. Sakalauskas, H. Behmenburg, P. Schley, G. Gobsch, C. Giesen, H. Kalisch, R. H. Jansen, M. Heuken, and R. Goldhahn, Phys. Status Solidi A **208**, 1517 (2011).

[34] F. Bassani and M. Altarelli, in *Handbook of Synchrotron Radiation*, edited by E. E. Koch (North-Holland, Amsterdam, 1983), Vol. 1.

[35] P. Y. Yu and M. Cardona, *Fundamentals of Semiconductors* (Springer, Berlin, 1996), pp. 251–253.

[36] A. Mang, K. Reimann, and S. Rübenacke, Solid State Commun. **94**, 251 (1995).

[37] Z. X. Liu, K. P. Korona, K. Syassen, J. Kuhl, K. Pakuła, J. M. Baranowski, I. Grzegory, and S. Porowski, Solid State Commun. **108**, 433 (1998).

[38] Strictly speaking, the exciton oscillator strength is proportional to the product $A \cdot \gamma$, but since we have fixed γ to a value independent of pressure, the following argument also holds as well for the Lorentz oscillator amplitude A alone.

[39] R. J. Elliott, Phys. Rev. **108**, 1384 (1957).

[40] A. R. Goñi, A. Cantarero, K. Syassen, and M. Cardona, Phys. Rev. B **41**, 10111 (1990).

[41] G. H. Li, A. R. Goñi, K. Syassen, and M. Cardona, Phys. Rev. B **49**, 8017 (1994).

[42] Q. X. Guo and A. Yoshida, Jpn. J. Appl. Phys. **33**, 2453 (1994).

[43] N. E. Christensen and I. Gorczyca, Phys. Rev. B **50**, 4397 (1994).

[44] R. Laskowski and N. E. Christensen, Phys. Status Solidi B **244**, 17 (2007).

[45] G. Rossbach, M. Röppischer, P. Schley, G. Gobsch, C. Werner, C. Cobet, N. Esser, A. Dadgar, M. Wieneke, A. Krost, and R. Goldhahn, Phys. Status Solidi B **247**, 1679 (2010).

[46] R. Schmidt-Grund, B. Rheinländer, E. M. Kaidashev, M. Lorenz, M. Grundmann, D. Fritsch, M. M. Schubert, H. Schmidt, and C. M. Herzinger, J. Korean Phys. Soc. **53**, 88 (2008).

[47] J. A. Van Vechten, Phys. Rev. **182**, 891 (1969).

[48] B. P. Singh, V. S. Baghel, and K. S. Baghel, Indian J. Pure Appl. Phys. **47**, 793 (2009).

[49] M. Alouani and J. M. Wills, Phys. Rev. B **54**, 2480 (1996).

[50] J.-M. Wagner and F. Bechstedt, Phys. Rev. B **62**, 4526 (2000).

[51] M. Fatmi, B. Ghebouli, M. A. Ghebouli, and Z. K. Hieba, Phys. Scr. **83**, 065702 (2011).

[52] P. Perlin, I. Gorczyca, N. E. Christensen, I. Grzegory, H. Teisseyre, and T. Suski, Phys. Rev. B **45**, 13307 (1992).

[53] P. Perlin, C. Jauberthie-Carillon, J. P. Itie, A. San Miguel, I. Grzegory, and A. Polian, Phys. Rev. B **45**, 83 (1992).

[54] J. Ibáñez, R. Oliva, F. J. Manjón, A. Segura, T. Yamaguchi, Y. Nanishi, R. Cuscó, and L. Artús, Phys. Rev. B **88**, 115202 (2013).

[55] R. Khenata, A. Bouhemadou, M. Sahnoun, A. H. Reshak, H. Baltache, and M. Rabah, Comput. Mater. Sci. **38**, 29 (2006).

[56] K. Vedam and E. D. D. Schmidt, Phys. Rev. **150**, 766 (1966).

[57] K. Vedam and T. A. Davis, Phys. Rev. **181**, 1196 (1969).

[58] K. Vedam and E. D. D. Schmidt, Phys. Rev. **146**, 548 (1966).

[59] P. G. Johannsen, G. Reiß, U. Bohle, J. Magiera, R. Müller, H. Spiekermann, and W. B. Holzapfel, Phys. Rev. B **55**, 6865 (1997).

[60] D. R. Penn, Phys. Rev. **128**, 2093 (1962).

[61] P. Nozières and D. Pines, Phys. Rev. **109**, 762 (1958).